Pion-nucleus elastic scattering at 80 MeV

M. J. Leitch, R. L. Burman, R. Carlini, S. Dam, and V. Sandberg
Los Alamos National Laboratory, Los Alamos, New Mexico 87545

M. Blecher, K. Gotow, and R. Ng*
Virginia Polytechnic Institute and State University, Blacksburg, Virginia 24061

R. Auble, F. E. Bertrand, E. E. Gross, F. E. Obenshain, and J. Wu†
Oak Ridge National Laboratory, Oak Ridge, Tennessee 37830

G. S. Blanpied, B. M. Preedom, and B. G. Ritchie‡
University of South Carolina, Columbia, South Carolina 29208

W. Bertozzi, M. V. Hynes,§ M. A. Kovash,** and R. P. Redwine
Massachusetts Institute of Technology, Cambridge, Massachusetts 02139
(Received 6 September 1983)

Differential cross sections for elastic scattering of 80 MeV positive and negative pions from ^{12}C, ^{40}Ca, ^{90}Zr, and ^{208}Pb were measured at 5° intervals for laboratory angles from 20° to 125°. These are compared with several optical model calculations.

I. INTRODUCTION

The study of low energy elastic pion scattering is important to the understanding of pion interactions with nuclei. At or near Δ resonance energies the elastic scattering of a pion can be described in terms of simple "black disc" or eikonal models, since the pion mean free path ($\lambda \sim 0.6$ fm) (Ref. 1) is fairly short and the scattering involves mainly the nuclear surface. At low energies (≤ 100 MeV), the pion interaction with the nucleus is relatively weak ($\lambda \sim 4$–6 fm)—hence nuclear matter appears to be more transparent. Consequently, the pion penetrates more deeply into the nucleus and a theoretical description of the scattering becomes much more complex. The simpler theories that are able to explain resonance energy scattering are no longer adequate. Thus far, only a relatively small body of low energy elastic scattering data exists[2]—in general, providing a survey of some common nuclei. Clearly, more low energy data are needed, especially in the transition region from resonance to low energy, near 80 MeV, where the complexities of low energy are just becoming important. In order to put sufficient constraints on the theories to allow the complicated pion-nuclear interaction to be unraveled, a variety of data are essential. These include elastic scattering on isotopes, single charge exchange, double charge exchange, and studies of other low energy pion reactions. Also needed is a good knowledge of the relevant nuclear structure as derived from other probes. Presented here are the results in the transition region at 80 MeV for π^+ and π^- elastic scattering angular distributions on ^{12}C, ^{40}Ca, ^{90}Zr, and ^{208}Pb.

At 80 MeV, the pion-nuclear interaction begins to take on the characteristics associated with resonance energy pions, but still retains the complications inherent at low energy. Energy differences, owing to Coulomb repulsion or attraction, are a substantial fraction of the pion energy and cause large shifts, between π^+ and π^-, of the minima in the angular distributions. The angular distributions contain a minimum, owing to the π-nucleon s- and p-wave interference, characteristic of low energy pion scattering, as well as diffraction minima owing to geometric effects, characteristic of resonance energy scattering.

At present, many optical model calculations can fit the data by varying parameters, but they are largely phenomenological and are difficult, if not impossible, to interpret in physical terms. A better calculation should contain a careful treatment of *all* the known first order ($\sim\rho \equiv$ nuclear density) contributions, hopefully without any adjustable parameters, to which adjustable second order ($\sim\rho^2$) terms can be added. One might then be able to deduce the physical character and importance of these second order contributions. Recently several theoretical efforts[3–6] have appeared that are parameter-free to first order. With these, it is possible to begin a study of the second order effects, bearing in mind that to express higher order corrections to an optical model in terms of ρ^2 is, at best, an oversimplification and that eventually a more sophisticated description is likely to become necessary.

II. EXPERIMENT

The experiment was done using the bicentennial spectrometer (BCS) on the low-energy pion channel[7] at the Clinton P. Anderson Meson Physics Facility (LAMPF) of the Los Alamos National Laboratory. Positive and negative pion beams with a momentum spread $\Delta P/P \simeq 0.5\%$ (FWHM) were used with pion fluxes of $\simeq 4.8\times10^7$ π^+/sec and $\simeq 1.2\times10^7$ π^-/sec. The beam spot on target was approximately 0.5 cm high and 2.5 cm wide with a

vertical divergence of 27 mrad and horizontal divergence of 40 mrad. Targets were self-supporting 5 cm by 13 cm sheets of the following thicknesses: CH_2-236 mg/cm^2, ^{12}C-226 mg/cm^2, ^{40}Ca-434 mg/cm^2, ^{90}Zr-120 mg/cm^2, and ^{208}Pb-154 mg/cm^2. These targets were mounted in the center of a 30 cm diam scattering chamber which was connected to the LEP channel vacuum. A 1 cm air gap and two 0.013 cm Kapton vacuum windows separated the scattering chamber from the BCS vacuum chamber.

The BCS magnetic spectrometer is a double focusing broad range device originally used at the Florida State University Tandem Van de Graaff Facility.[8] New coils were installed and the pole gap was increased from 2.5 to 5.0 cm in order to obtain a solid angle of 6 msr for this work. The central trajectory length is only two meters long, thus holding pion decay losses to less than 20% at 80 MeV. As shown in Fig. 1, scattered pions enter through the solid angle defining slits, just inside the front vacuum window, and are bent upward through $\sim 90°$ onto a focal plane which is tilted at approximately 45° with respect to the horizontal. The focal plane detector array consists of a vertical drift chamber (VDC) behind which are two long scintillators with phototubes on both ends. The VDC is a larger version of the VDC used in electron scattering experiments at the MIT-Bates electron linac as described elsewhere.[9] It has an active area of 135 cm in length and 22.5 cm in width and covers a 50% range in momentum. A pion traverses the chamber at an angle of $\gtrsim 45°$ relative to the normal to the plane of the chamber, as shown in Fig. 2, and will hit four or more of the drift cells which are normal to the plane of the chamber. As outlined in the figure, measurements of the several drift times allows the position and angle to be determined. An intrinsic accuracy of 0.1 mm variance in position and 12 mrad variance in angle is obtained. The signal from each wire of the chamber is passed to one of fourteen interleaved delay lines in order to allow up to fourteen hits for one track. The difference in the times from the two ends of each delay line gives the wire number, and the sum of the two times gives the drift time.

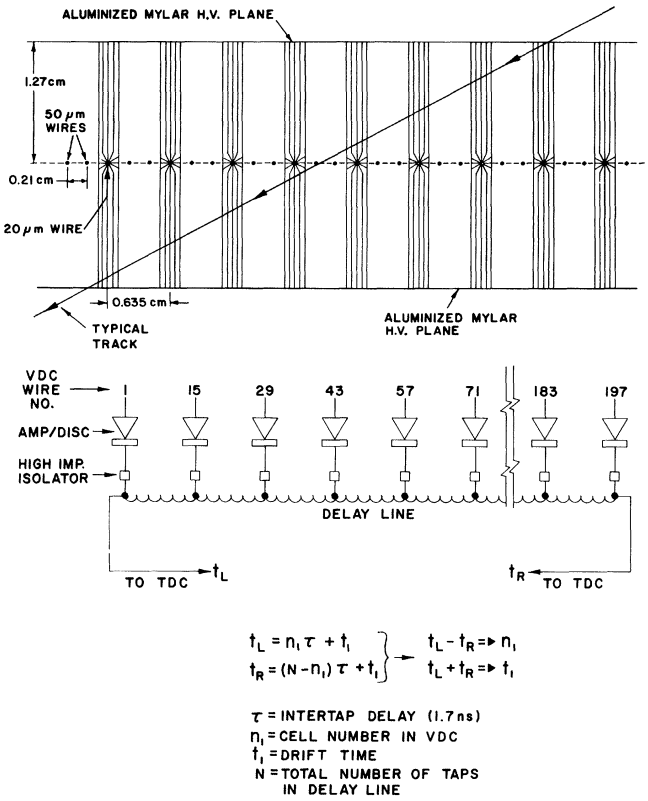

FIG. 2. (a) Cross section of the VDC showing geometry, field lines, and a typical track. Sense wires are 20 μm in diameter and field shaping wires 50 μm. (b) Delay-line readout scheme. Shown is one of the 14 interleaved delay lines, the next delay line is attached to sense wires 2, 16, 30, . . . , and 198, etc.

Signals from two 0.64 cm thick scintillators ($S1$,$S2$), 20

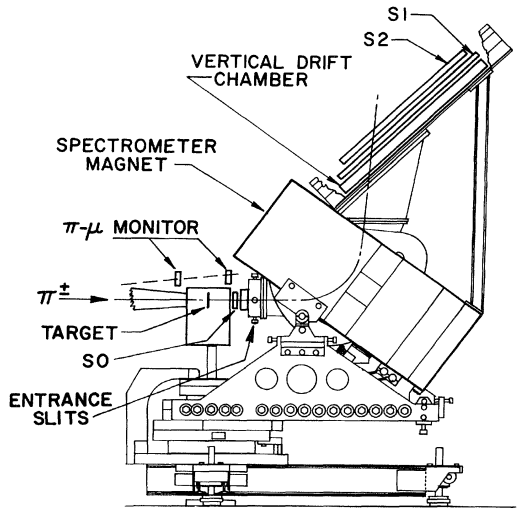

FIG. 1. The bicentennial spectrometer system. It consists of a single dipole magnet with an event trigger system of three scintillators, $S0$ at the magnet entrance and $S1$ and $S2$ behind the focal plane, and a vertical drift chamber (VDC) lying along the focal plane. The VDC measures position and angle in the focal plane with a single wire plane. The π-μ monitor is a scintillator telescope used to monitor the incident pion flux.

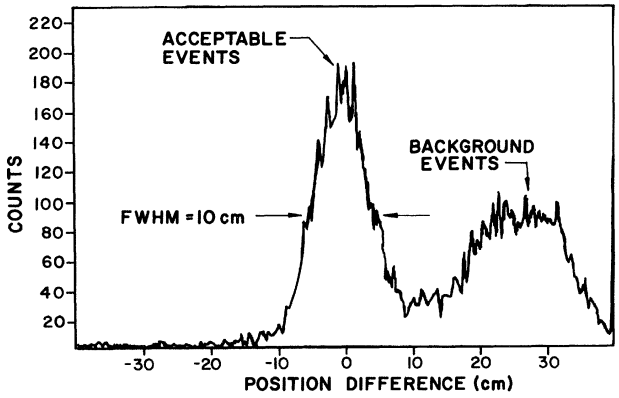

FIG. 3. Resolution of the angle ambiguity in the VDC. Shown is the difference between the position on the scintillator plane determined by scintillator timing and that determined by projection of the VDC trajectory. Particles transversing the spectrometer are in the peak at zero position difference; background particles typically have large nonzero position differences.

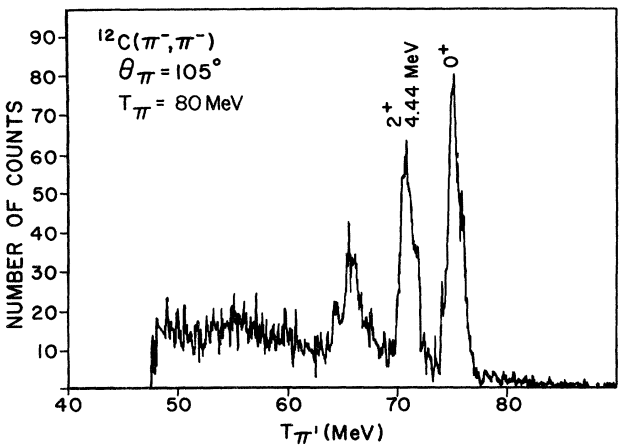

FIG. 4. Typical kinetic energy spectrum. Shown is the spectrum of π^- scattered from ^{12}C.

cm in width and of lengths 170 and 155 cm, along with a thin (0.16 cm) scintillator ($S0$) at the spectrometer entrance, provide a trigger for the system. The VDC can determine only the magnitude of the angle relative to its normal, but not its sign. To determine the sign, the timing signals from the two ends of $S1$ and of $S2$ are used to determine the position to an accuracy of ± 5 cm. This is compared to the position in the scintillators, as projected by the VDC, to resolve the ambiguity in sign. A large amount of background from the main proton beamline that has angles inconsistent with a trajectory through the spectrometer is rejected as indicated in Fig. 3.

The data acquisition system consists of a fast NIM electronic logic system to form the trigger, CAMAC analog-to-digital converters (ADC's) and time-to-digital converters (TDC's) to collect pulse areas and times, and an MBD (microprogrammed branch driver) that interfaces the CAMAC to a PDP 11/45. The trigger requires a signal on both ends of $S1$ and $S2$, as well as a signal from $S0$. A standard LAMPF data acquisition software system[10] reads the data from the CAMAC via the MBD, writes it onto magnetic tape, and processes it for on line inspection.

To extract cross sections from the data, first elastically scattered pion yields were obtained. A typical spectrum is shown in Fig. 4. All elastic pion peaks were placed in the same position on the focal plane to avoid errors owing to solid angle variation over the focal plane. Pion yields were obtained by fitting the elastic peaks in the pion energy spectrum with a Gaussian peak shape. The ^{40}Ca target was partially oxidized. A long run at 90° was used to determine the contamination to be $\cong 3\%$ by atom. The ^{40}Ca data at other angles were then corrected for this contamination using the known ^{16}O cross sections.[11] Yields were then corrected for pion decay in the spectrometer according to the momentum of the scattered pion and the fixed distance (2.15 m) between the target and the elastic peak in the focal plane. Scattering of electrons and muons are indistinguishable from scattering of pions for our detection system. Corrections for this were made but are important only at small scattering angles and for high Z targets. The relative flux of electrons and muons to pions was taken from previous measurements:[12]

$$\mu^+/\pi^+ \simeq 0.11, \quad \mu^-/\pi^- \simeq 0.08 ,$$

$$e^+/\pi^+ \simeq 0.08, \quad e^-/\pi^- \simeq 0.43 .$$

(These ratios have $\sim 20\%$ systematic uncertainty owing to different pion beam tunes.) The elastic electron scattering cross sections were obtained from phase shift fits to electron scattering data and scaled with the appropriate form factor to obtain muon scattering cross sections. The largest correction was $\sim 14\%$ for Pb at 20°.

Absolute normalization was obtained by comparison of $\pi^\pm$-nuclear scattering yields with $\pi^\pm$-hydrogen scattering. The relative number of pions was obtained from a pion decay telescope, labeled as the π-μ monitor in Fig. 1. Table I gives the $\pi^\pm$-proton elastic scattering cross sections used for normalization. The π^+p cross sections are an interpolation of the data of Bertin *et al.*,[13] at 67.4 and

TABLE I. π^+p and π^-p cross sections used in absolute normalization.

π nuclear data	πp cross section (mb/sr)
π^+,C,Ca	$\sigma(\pi^+p)=2.51 \pm 0.07$ at $\theta_{lab}=94.7°$
π^+,Zr,Pb	$\sigma(\pi^+p)=1.58 \pm 0.07$ at $\theta_{lab}=55.2°$
π^-,all	$\sigma(\pi^-p)=0.552 \pm 0.056$ at $\theta_{lab}=55.2°$

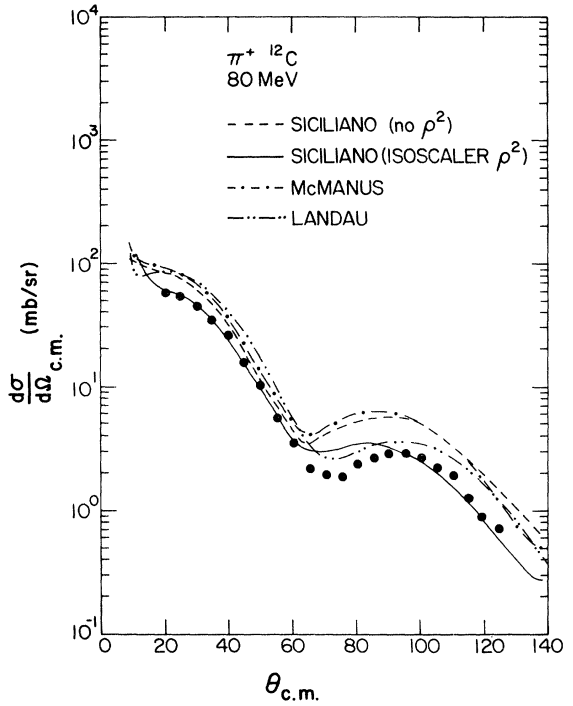

FIG. 5. Differential cross sections for elastic scattering of π^+ on ^{12}C. The data are shown as filled circles, with errors typically less than the size of the circle. The various optical model calculations are discussed in the text: the dashed and solid curves are from Siciliano, the dotted-dashed curve from Stricker, McManus, and Carr, and the dotted-dotted-dashed curve from Landau and Thomas.

TABLE II. Differential cross sections for π^+-nucleus elastic scattering at 80 MeV. Scattering angles and cross sections are in the center of mass with units of degrees and mb/sr, respectively.

^{12}C			^{40}Ca			^{90}Zr			^{208}Pb		
$\theta_{c.m.}$	$\frac{d\sigma}{d\Omega_{c.m.}}$	$\Delta\sigma_{c.m.}$	$\theta_{c.m.}$	$\frac{d\sigma}{d\Omega_{c.m.}}$	$\Delta\sigma_{c.m.}$	$\theta_{c.m.}$	$\frac{d\sigma}{d\Omega_{c.m.}}$	$\Delta\sigma_{c.m.}$	$\theta_{c.m.}$	$\frac{d\sigma}{d\Omega_{c.m.}}$	$\Delta\sigma_{c.m.}$
20.4	57.40	2.25	20.1	306.86	16.57	20.1	585.83	19.76	20.0	1107.34	50.14
25.5	53.84	2.00	25.1	223.33	9.95	25.1	392.90	14.96	25.0	681.58	29.59
30.6	45.07	2.35	30.2	166.08	9.42	30.1	200.24	7.19	30.0	190.25	10.33
35.6	34.25	1.92	35.2	95.76	5.25	35.1	87.16	4.67	35.0	24.44	4.42
40.7	25.51	1.28	40.2	49.41	1.93	40.1	23.88	2.39			
45.8	15.76	0.64	45.2	21.31	1.61	45.1	4.75	0.80	45.1	19.90	1.08
50.9	9.82	0.49	50.3	8.49	0.71	50.1	4.79	0.58	50.1	25.24	1.24
55.9	5.65	0.30	55.3	4.55	0.28	55.1	8.00	0.64	55.1	16.89	1.04
61.0	3.50	0.21	60.3	4.77	0.22	60.1	8.91	0.67	60.1	5.41	0.53
66.0	2.18	0.12	65.3	5.23	0.19	65.1	5.10	0.42	65.1	2.17	0.42
71.0	1.91	0.10	70.3	4.26	0.17	70.1	1.97	0.15	70.1	3.18	0.36
76.1	1.88	0.09	75.3	3.19	0.21	75.1	0.76	0.17	75.1	4.30	0.38
81.1	2.38	0.10	80.3	1.53	0.12	80.1	1.44	0.18	80.1	3.06	0.22
86.1	2.66	0.10	85.3	0.49	0.07	85.1	2.72	0.24	85.1	0.92	0.09
91.1	2.85	0.11				90.1	3.75	0.30			
96.1	2.91	0.11	95.3	0.20	0.05	95.1	3.43	0.27	95.1	1.12	0.15
101.1	2.68	0.10	100.3	0.85	0.04	100.1	2.67	0.25	100.1	2.97	0.33
106.1	2.21	0.09	105.3	1.70	0.08	105.1	1.64	0.15	105.1	3.61	0.26
111.0	1.94	0.09	110.3	2.32	0.08	110.1	0.99	0.05	110.1	3.58	0.23
116.0	1.27	0.08	115.3	2.71	0.03	115.1	0.94	0.07	115.1	2.67	0.24
121.0	0.88	0.05	120.3	2.62	0.10	120.1	0.65	0.10	120.1	2.14	0.12
125.9	0.72	0.05	125.3	2.41	0.11						

81.7 MeV. The π^-p cross sections are obtained by using the Zidell, Arndt, and Roper[14] phase shifts to obtain the ratio

$$\sigma(\pi^+\text{p},55.2°)/\sigma(\pi^-\text{p},55.2°)=2.86\pm10\% \ .$$

This ratio was used to scale the π^+p cross sections to obtain an estimated π^-p cross section.

The π-μ monitor measured the relative number of pions for each data run by detecting decay muons. It consisted

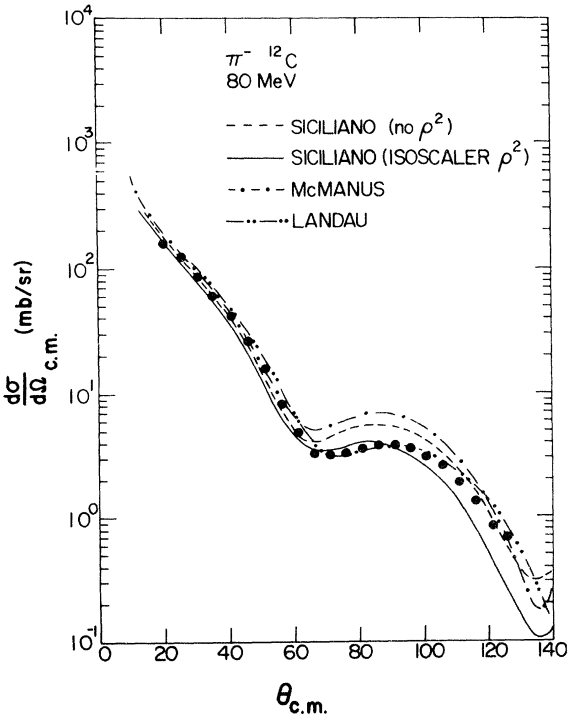

FIG. 6. Differential cross sections for elastic scattering of π^- on ^{12}C. The curves have the same definition as in Fig. 5.

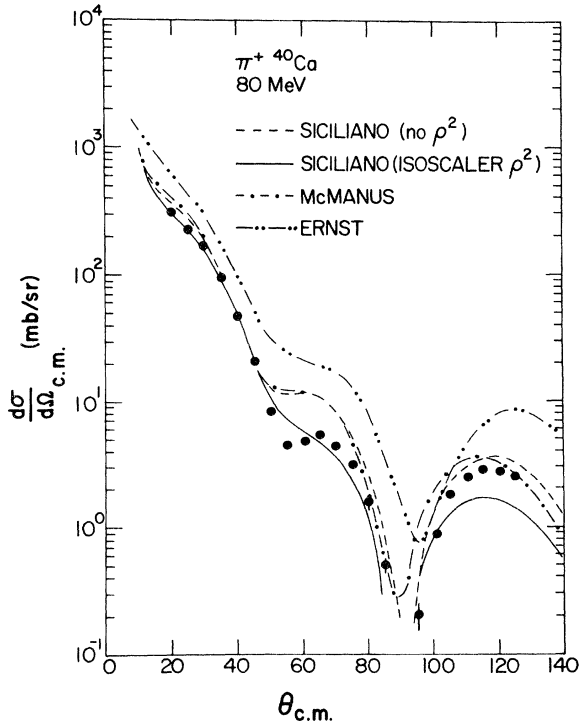

FIG. 7. Differential cross sections for elastic scattering of π^+ on ^{40}Ca. The curves have the same definition as in Fig. 5.

TABLE III. Differential cross sections for π^--nucleus elastic scattering at 80 MeV. Scattering angles and cross sections are in the center of mass with units of degrees and mb/sr, respectively.

^{12}C			^{40}Ca			^{90}Zr			^{208}Pb	
$\theta_{c.m.}$	$\frac{d\sigma}{d\Omega_{c.m.}}$	$\Delta\sigma_{c.m.}$	$\theta_{c.m.}$	$\frac{d\sigma}{d\Omega_{c.m.}}$	$\Delta\sigma_{c.m.}$	$\theta_{c.m.}$	$\frac{d\sigma}{d\Omega_{c.m.}}$	$\Delta\sigma_{c.m.}$	$\theta_{c.m.}$	$\frac{d\sigma}{d\Omega_{c.m.}}$	$\Delta\sigma_{c.m.}$
20.4	158.02	6.56	20.1	816.57	38.67	20.1	1374.48	96.15	20.0	1998.05	188.91
25.5	123.23	5.16	25.1	469.39	22.54	25.1	591.12	34.32	25.0	444.30	45.40
30.6	86.94	4.57	30.2	260.57	9.68	30.1	230.42	16.37	30.0	183.84	13.71
35.6	60.26	3.16	35.2	136.97	6.61	35.1	78.87	6.20	35.0	210.80	12.09
40.7	41.82	2.44	40.2	66.59	3.42	40.1	49.78	3.28	40.0	163.75	9.24
45.8	26.43	1.45	45.2	31.82	1.94	45.1	59.20	3.97	45.1	80.16	4.10
50.9	15.81	0.91	50.3	18.48	1.28	50.1	48.81	2.90	50.1	30.09	2.55
55.9	8.32	0.51	55.3	17.79	0.96	55.1	34.80	2.33	55.1	24.59	1.83
61.0	4.82	0.30	60.3	16.37	0.92	60.1	16.64	1.30	60.1	33.26	2.25
66.0	3.36	0.21	65.3	13.56	0.74	65.1	8.51	0.82	65.1	20.76	1.28
71.0	3.16	0.18	70.3	9.39	0.46	70.1	7.46	0.71	70.1	7.71	0.71
76.1	3.25	0.13	75.3	5.28	0.33	75.1	11.07	0.83	75.1	3.58	0.70
81.1	3.60	0.22	80.3	2.43	0.18	80.1	12.19	1.06	80.1	8.64	0.89
86.1	3.85	0.20	85.3	1.10	0.13	85.1	8.91	0.94	85.1	10.46	1.01
91.1	3.83	0.20	90.3	1.18	0.08	90.1	4.55	0.45	90.1	6.71	0.67
96.1	3.56	0.29	95.3	1.77	0.11	95.1	1.03	0.17	95.1	1.37	0.37
101.1	3.06	0.16	100.3	2.53	0.15						
106.1	2.62	0.13	105.3	3.29	0.16	105.1	1.53	0.17	105.1	3.03	0.30
111.0	1.90	0.08	110.3	3.65	0.20	110.1	3.60	0.33	110.1	5.24	0.55
116.0	1.30	0.05	115.3	3.32	0.24	115.1	4.22	0.38	115.1	4.58	0.53
121.0	0.84	0.05	120.3	2.38	0.10	120.1	4.31	0.45	120.1	2.62	0.42
125.9	0.66	0.04	125.3	1.16	0.14	125.1	3.83	0.29			

of a scintillator telescope composed of two 1.27 cm diam 0.318 cm thick counters set 30.5 cm apart at an angle well inside the Jacobian peak for pion decay.[15] This monitor was found to be insensitive to small changes in the direction and momentum spread of the pion beam.

Finally, the angular distributions were corrected for finite solid angle effects. Phase shift fits to the uncorrected laboratory cross sections were used to obtain first and second derivatives of the cross section with respect to an-

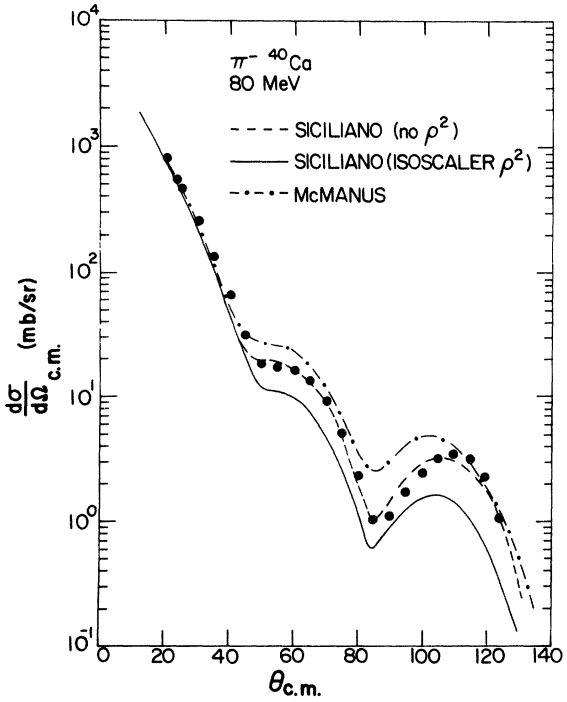

FIG. 8. Differential cross sections for elastic scattering of π^- on ^{40}Ca. The curves have the same definition as in Fig. 5.

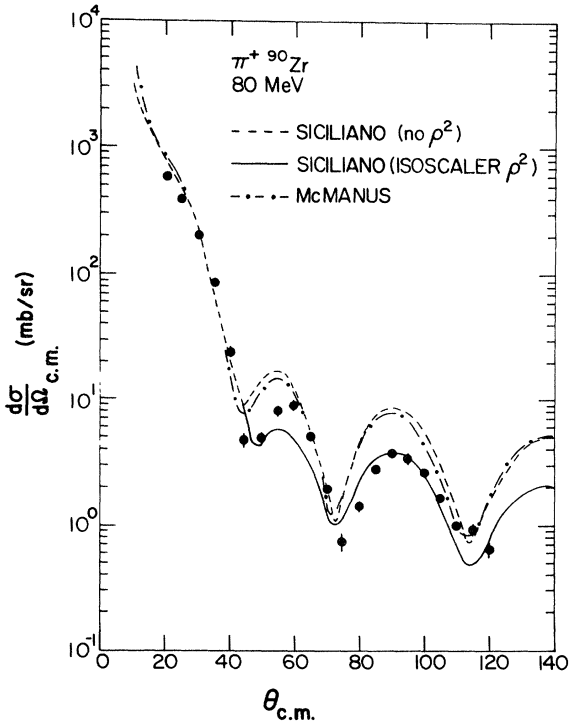

FIG. 9. Differential cross sections for elastic scattering of π^+ on ^{90}Zr. The curves have the same definition as in Fig. 5.

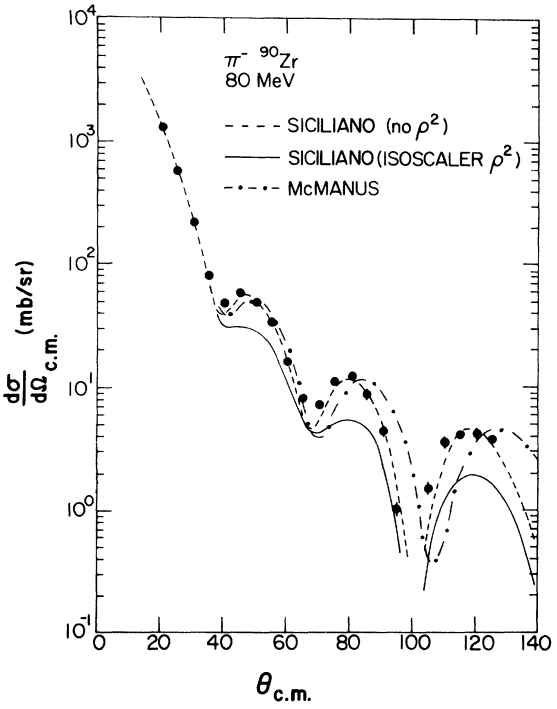

FIG. 10. Differential cross sections for elastic scattering of π^- on ^{90}Zr. The curves have the same definition as in Fig. 5.

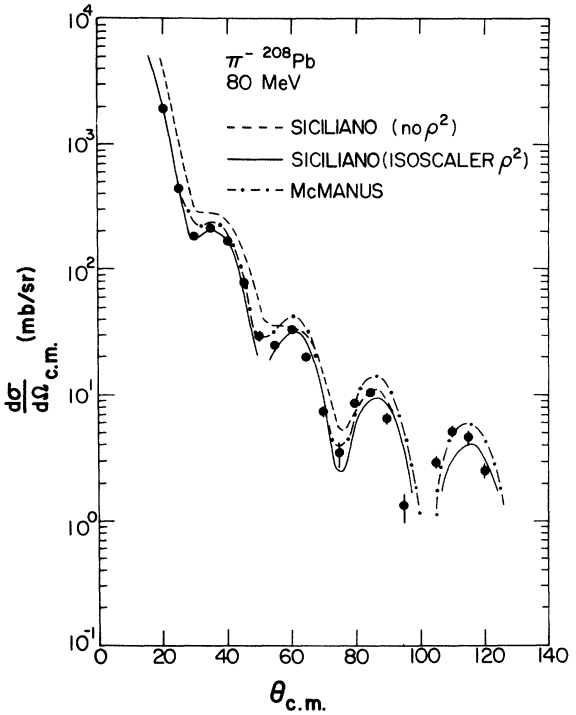

FIG. 12. Differential cross sections for elastic scattering of π^- on ^{208}Pb. The curves have the same definition as in Fig. 5.

gle; these derivatives were then used in analytic calculations of the finite solid angle corrections. The effect of the correction is a reduction of the cross sections at very forward angles and a deepening of the minima. Cross sections requiring a correction larger than 50% were removed from the data set.

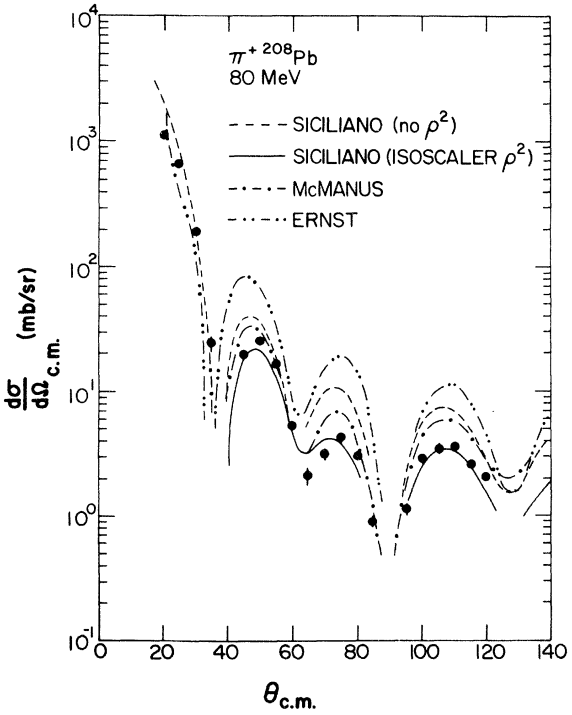

FIG. 11. Differential cross sections for elastic scattering of π^+ on ^{208}Pb. The curves have the same definition as in Fig. 5.

III. DATA

The π^+ and π^- elastic scattering angular distributions are shown in Figs. 5—12 and tabulated in Tables II and III. Relative uncertainties listed include the statistical error in the yield for the measured cross section. The ^{40}Ca cross sections contain an additional uncertainty owing to oxygen contamination in the target which varies according to the relative ^{40}Ca and ^{16}O cross sections at the various angles. Finite solid angle corrections were made for the horizontal and vertical size of the spectrometer solid angle slits, the beam spot on target, the beam divergence on target, and the multiple scattering in the target. The uncertainty owing to the finite solid angle correction was taken to be 20% of the magnitude of the correction. Overall systematic uncertainties are the following: 6.8% for (π^+,^{12}C); 9.0% for (π^+,^{40}Ca); 10.1% for (π^+,^{90}Zr) and (π^+,^{208}Pb); and 10.5% for all the π^- data.

IV. INTERPRETATION

At present our understanding of low energy pion scattering is largely in terms of various optical model calculations. These calculations use phase shift fits to π-nucleon scattering to obtain the free π-nucleon t matrix[16] and fold this into a multiple scattering theory to describe the π-nucleus interaction.[17] At low energies both the s- and p-wave parts of the π-nucleon interaction are important in contrast to resonance energies where the p-wave dominates. The t matrix is modified to account for Pauli blocking in the nucleus. The energy at which it is evaluated is modified according to the Fermi motion of the nucleons and the Coulomb attraction or repulsion of the nucleus. Lorentz-Lorenz terms,[18] which are included in

some of the calculations, seem to be important at low energies. The choice of different forms of the nuclear density does not seem to be important for elastic scattering. In addition, effects such as true pion absorption or Δ-nuclear dynamics,[19] which do not naturally enter through the π-nucleon t matrix, can be included given an appropriate model.

The practical approach taken now attempts to include all the π-nuclear physics that we know about as a "first order" calculation and then explore the need for any additional "second order" terms, attempting to understand these in terms of physical models. For example, at low energies true pion absorption is generally accepted as playing an important part in the reaction mechanism, so we can study the need for optical model terms which could represent true absorption. It is extremely important to be sure that the first order is done correctly before inferring that disagreement between the first-order calculation and the data implies the presence of a new physical phenomenon. We now describe the results of several available calculations in comparison with this data.

Landau and Thomas have done a first order optical model calculation with no adjustable parameters. The details of their calculation are described in Ref. 3. Their calculation contains a Pauli modified $t_{\pi N}$, an exact treatment of the Coulomb interaction, three-body energies, and uses harmonic oscillator wave functions. The results are shown in Fig. 5 for π^+ and π^- elastically scattered on ^{12}C. The magnitude of the data is generally well predicted (especially for π^-), as are the locations of the minima.

Sticker, McManus, and Carr have started with an optical model calculation based upon a fit to pionic atom data and have then extended it to higher energies using the energy dependence of the π-nucleon phase shifts.[4] Shown in Fig. 5 are calculations for π^+ and π^- on ^{12}C, ^{40}Ca, ^{90}Zr, and ^{208}Pb. The calculations tend to be high by roughly a factor of 2 for all the secondary maxima. Also, the predicted position of the minima tends to be small for π^+ scattering and too large for π^- scattering. However, this is a low energy theory and accuracy at 80 MeV would be surprising.

Ernst[5] has done a momentum-space first-order optical model calculation with complete relativistic kinematics. The Lorentz-Lorenz terms which are included in other calculations (see Siciliano below) have been left out. Results are shown for π^+ scattering on ^{40}Ca and ^{208}Pb in Fig. 5. The location of the minima are well predicted, but the magnitude of the calculation is generally too high by a factor of 2 or more except at small angles for ^{208}Pb where Coulomb scattering dominates the cross section.

Siciliano has made his optical model program, PIESDEX, available to us.[6] This coordinate-space calculation, which includes both π-nucleon s and p waves and the Coulomb potential, has isoscalar, isovector, and isotensor parts. It can use parametrized densities such as a three-parameter Fermi density or it can read in tabulated densities. We have used tabulated DME (density matrix expansion) densities.[20] The first-order terms ($\sim\rho$) of the optical potential are determined from the pion-nucleon phase shifts. Phenomenological ρ^2 (second order) terms can be turned on in the calculation to investigate the need for, or sensitivity to, these ρ^2 terms. The calculation also includes a representation of the Lorentz-Lorenz effect in the p wave and an increased isoscalar s-wave repulsion.[4] Siciliano is in the process of improving and extending the treatment of the Lorentz-Lorenz effects.

Shown in Fig. 5 are the results of calculations with PIESDEX compared to our 80 MeV elastic scattering data. The solid curve is the parameter-free first-order calculation and the dashed curve includes, in addition, a phenomenological ρ^2 p-wave isoscalar piece which had been found to produce good agreement for elastic scattering on ^{16}O at 50 MeV.[6] This term can be considered as representing true absorption; the value used in the calculations corresponds to typical pionic atom values.[4] We make no attempt here to fit the data by varying the ρ^2 parameters. The first order calculation is generally somewhat high ($\sim$50%) for π^+, but very close in magnitude to the data for π^-, especially for larger A. The minima are well predicted except perhaps for ^{12}C. With the addition of the ρ^2 term, the π^+ calculation is now rather close and the π^- somewhat low.

V. CONCLUSIONS AND SUMMARY

Presented here are angular distributions for π^+ and π^- elastic scattering at 80 MeV for several closed-shell nuclei: ^{12}C, ^{40}Ca, ^{90}Zr, and ^{208}Pb. The distortions of the pion wave by the nucleus obtained from these elastic scattering measurements are essential to the interpretation of pion inelastic scattering. A separate paper presents inelastic scattering results obtained by this group.[21] These data are important in the understanding of the complicated pion-nucleus interaction at low energies, which at present is generally advanced within the framework of various optical models. Some parts of the pion-nucleus interaction, which are buried underneath (3,3) resonance contributions at resonance energies, become available for study at low energies (for example, true absorption).

Since sensitivities to nonisoscalar and higher order parts of the optical potential are minimal for elastic scattering from even-even nuclei there is a great need for complementary data. A study of the isotope (or isotone) dependence of elastic scattering would contribute to an understanding of the isovector parts of the π-nucleus interaction. Pion single- and double-charge exchange to isobaric analog states at low energies is very important to complete the picture and should serve to constrain the isovector, isotensor, and higher order ($\sim\rho^2$) parts of the optical potential.

ACKNOWLEDGMENTS

The authors are indebted to LAMPF for the technical support we have received during the course of this experiment. We thank R. H. Landau, H. McManus, D. J. Ernst, and E. R. Siciliano for providing their optical model calculations. This research was supported by the U.S.

Department of Energy (Los Alamos National Laboratory and Massachusetts Institute of Technology), by the Division of High Energy and Nuclear Physics, U.S. Department of Energy, under contract W-7405-eng-26 with the Union Carbide Corporation (Oak Ridge National Laboratory), and by the National Science Foundation (Virginia Polytechnic Institute and State University, and University of South Carolina).

---

*Present address: Purdue University, West Lafayette, IN 47907.
†Present address: Bell Labs, Naperville, IL 60540.
‡Present address: University of Maryland, College Park, MD 20742.
§Present address: Los Alamos National Laboratory, Los Alamos, NM 87545.
**Present address: University of Kentucky, Lexington, KY 40506.

[1]P. Hecking, Phys. Lett. 103B, 401 (1981).
[2]B. M. Preedom, *Proceedings of the 7th International Conference on High Energy Physics and Nuclear Structure, Zürich, 1977,* edited by M. P. Locher (Birkhauser, Basel, 1977), p. 119; R. P. Redwine, *Meson-Nuclear Physics—1979 (Houston), Proceedings of the 2nd International Topical Conference on Meson-Nuclear Physics,* AIP Conf. Proc. No. 54, edited by E. V. Hungerford III (AIP, New York, 1979).
[3]A. W. Thomas and R. H. Landau, Phys. Rep. 58, 121 (1980).
[4]K. Striker, H. McManus, and J. A. Carr, Phys. Rev. C 19, 929 (1979); 22, 2043 (1980).
[5]D. J. Ernst (private communication).
[6]E. R. Siciliano (private communication); M. B. Johnson and E. R. Siciliano, Phys. Rev. C 27, 730 (1983); 27, 1647 (1983).
[7]R. L. Burman, R. L. Fulton, and M. Jakobson, Nucl. Instrum. Methods 131, 29 (1975).
[8]A. E. S. Green, R. J. Berkley, C. E. Watson, and C. F. Moore, Rev. Sci. Instrum. 37, 415 (1966).
[9]W. Bertozzi, M. V. Hynes, C. P. Sargent, C. Creswell, P. C. Dunn, A. Hirsch, M. Leitch, B. Norum, F. N. Rad, and T. Sasanuma, Nucl. Instrum. Methods 141, 457 (1977).
[10]D. G. Perry, IEEE Trans. Nucl. Sci. NS-26, No. 4 (1979).
[11]J. P. Albanese, J. Arvieux, J. Bolger, E. Boschitz, C. H. Q. Ingram, J. Jansen, and J. Zichy, Nucl. Phys. A350, 301 (1980); R. M. Edelstein, W. F. Baker, and J. Rainwater, Phys. Rev. 122, 252 (1961).
[12]J. S. Frank (private communication); Phys. Rev. D 28, 1569 (1983).
[13]P. Y. Bertin, B. Coupat, A. Hivernat, P. B. Isabelle, J. Duclos, A. Gerard, J. Miller, J. Morgenstern, J. Picard, P. Vernin, and R. Powers, Nucl. Phys. B106, 341 (1976).
[14]V. S. Zidell, R. A. Arndt, and L. D. Roper, Phys. Rev. D 21, 1255 (1980).
[15]E. A. Wadlinger, Nucl. Instrum. Methods 134, 243 (1976).
[16]G. Rowe, M. Salomon, and R. H. Landau, Phys. Rev. C 18, 584 (1978).
[17]*Theoretical Methods in Medium Energy and Heavy Ion Physics,* edited by K. W. McVoy and W. A. Friedman (Plenum, New York, 1978).
[18]W. R. Gibbs, B. F. Gibson, and G. J. Stephenson, Phys. Rev. Lett. 39, 1316 (1977); J. M. Eisenberg, J. Hüfner, and E. J. Moniz, Phys. Lett. 47B, 381 (1973).
[19]M. Hirata, J. H. Koch, F. Lenz, and E. J. Moniz, Ann. Phys. (N.Y.) 120, 205 (1979).
[20]J. W. Negele, Phys. Rev. C 1, 1260 (1970).
[21]M. Blecher, K. Gotow, R. Ng, R. L. Burman, R. Carlini, S. Dam, M. V. Hynes, M. J. Leitch, V. Sandberg, R. Auble, F. E. Bertrand, E. E. Gross, F. E. Obenshain, J. Wu, G. S. Blanpied, B. M. Preedom, B. G. Ritchie, W. Bertozzi, M. A. Kovash, and R. P. Redwine, Phys. Rev. C 25, 2554 (1982).